Effects of Alloying Elements upon Austenite Decomposition in Low-C Steels

J.K. CHEN, R.A. VANDERMEER, and W.T. REYNOLDS, JR.

The kinetics of austenite decomposition were studied in high-purity Fe-0.1C-0.4Mn-0.3Si-*X* (concentrations in weight percent; *X* represents 3Ni, 1Cr, or 0.5Mo) steels at temperatures between 500 °C and 675 °C. The transformation stasis phenomenon was found in the Fe-C-Mn-Si-Mo and Fe-C-Mn-Si-Ni alloys isothermally transformed at 650 °C and 675 °C but not in the Fe-C-Mn-Si and Fe-C-Mn-Si-Cr alloys at any of the temperatures investigated. The occurrence of transformation stasis was explained by synergistic interactions among alloying elements. The paraequilibrium model was applied to calculate the metastable fraction of ferrite in each alloy. This fraction was shown to coincide with cessation of transformation in the Mo alloy transformed at 600 °C. Transformation stasis was found in both the Ni and the Mo alloys isothermally reacted at 650 °C and 675 °C. The interactions among Mn, Si, and Mo, as well as interactions among Mn, Si, and Ni, appear to decrease the threshold concentrations for transformation stasis in Fe-C-Mn-Si systems. Segregation of Mn and Mo to the α/γ boundary, assisted by the presence of Si, was suggested to enhance the solute draglike effect (SDLE) and lead to transformation stasis. In the Ni alloy, a lower driving force for ferrite formation resulting from the Ni addition could be responsible for the occurrence of transformation stasis.

I. INTRODUCTION

THE overall kinetics of austenite decomposition have been investigated previously in a series of ternary steels including Fe-C-Mo,[1,2] Fe-C-Cr,[3] Fe-C-Ni,[4] Fe-C-Mn,[4,5,6] Fe-C-Cu,[4] and Fe-C-Si.[4,5,6] These efforts emphasized the effects of the substitutional alloying elements upon the morphology and the kinetics of ferrite formation. It was found that the incomplete transformation phenomenon, often presumed to be characteristic of the bainite reaction,[7] is absent in many ternary alloys. The occurrence of incomplete transformation, or transformation stasis,[8] required minimum concentrations of C and Mo, Cr, or Mn. It was not observed in Fe-C-Ni or Fe-C-Si alloys. Since many commercial steels exhibit time-temperature-transformation (TTT) diagrams that suggest the possibility of transformation stasis, it is possible that occurrence of this phenomenon is enhanced by interactions among substitutional alloying elements. Some data from Fe-C-Mn-Si alloys support this view.[5,6,9,10]

It has been recognized for some time that TTT diagrams of plain C steels exhibit a single *C* curve, and some high-alloy steels have two *C* curves.[7] The two *C* curves result from a change with temperature in the mechanisms of ferrite formation.[2] The change in mechanism with decreasing reaction temperature occurs at a characteristic temperature designated as the bay temperature, T_b. This is the temperature at which the two *C* curves for initiation of transformation intersect. The bay temperature has also been called the bainite start temperature.[7] However, this usage is often ambiguous,[4,5,11,12] so it will not be employed here.

J.K. CHEN, Graduate Student, and W.T. REYNOLDS, Jr., Associate Professor, are with the Materials Science and Engineering Department, Virginia Polytechnic Institute and State University, Blacksburg, VA 24061-0237. R.A. VANDERMEER, Branch Consultant, is with the Physical Metallurgy Branch, Naval Research Laboratory, Washington, DC 20375-5000.

Manuscript submitted September 3, 1993.

During transformation stasis,[8] both ferrite nucleation and growth stop completely, and the fraction transformed displays a plateau when plotted *vs* the logarithm of the reaction time. Cessation of ferrite formation can result from thermodynamic or kinetic factors. From a thermodynamic standpoint, transformation can cease when the metastable fraction of ferrite forms in the absence of carbide precipitation.[1] This fraction of ferrite can be predicted using thermodynamic models.

If cessation of ferrite formation occurs before the metastable fraction is reached, then the cause must be kinetic in origin. The term "transformation stasis" is used to refer to this form of cessation. Investigations of Fe-C-X alloys have led to the view that transformation stasis,[2,3,4,13] as well as anomalously slow ferrite growth kinetics[1,14,15,16] and highly degenerate ferrite morphologies,[2,16,17] can be ascribed to a solute draglike effect (SDLE).[11,18,19] An alternate hypothesis based upon a displacive transformation mechanism has also been used to explain transformation stasis. A recent summary of this model, which is not used here, is available in Reference 20, and a discussion of its feasibility can be found in Reference 12.

On the SDLE hypothesis, nonequilibrium absorption of a substitutional alloying element occurs to ferrite/austenite boundaries. When the element is one that markedly reduces the activity of C, the effective C concentration gradient in austenite ahead of a growing ferrite crystal is reduced. Since this gradient is responsible for driving ferrite growth, absorption of the solute element reduces ferrite growth kinetics. In extreme cases, ferrite growth ceases altogether.

Transformation stasis can be explained by considering the influence of the SDLE upon ferrite growth, together with the change in the mechanism of ferrite nucleation at the bay temperature.[2] At temperatures below T_b, ferrite growth is greatly restricted by the SDLE. Transformation proceeds by the nucleation of a ferrite crystal on

a pre-existing ferrite grain (sympathetic nucleation[21]), followed by a limited amount of growth. Once the SDLE inhibits the growth of the sympathetically nucleated crystal, a new ferrite crystal nucleates and grows until the SDLE inhibits migration of its boundaries. However, since ferrite growth is accompanied by C partitioning, the driving force for sympathetic nucleation rapidly declines with the amount of ferrite formed. Transformation stasis begins when there is no longer sufficient driving force to support sympathetic nucleation of ferrite. Transformation does not resume until carbides form, and the driving force for ferrite nucleation and growth is restored.[2,4]

Four types of overall reaction kinetics behavior (Figure 1) were observed in alloys presumed to have a strong SDLE.[13] When austenite transformation ceases completely below the metastable ferrite fraction (transformation stasis), the transformation curve shows a zero slope. This is recognized as type IV transformation. At lower temperatures or in materials with lower concentrations of C and alloying elements, transformation is impeded but does not stop completely, resulting in type II and type III transformation behaviors. Type I transformation results from little or no SDLE, and it also appears at temperatures above T_b.

In four or more component steels, the SDLE is likely to be complicated by interactions among the alloying elements, but the nature of these interactions is not yet clear. In recent work on the nucleation and growth of ferrite in an Fe-C-Mn-Si alloy, no strong interaction between Mn and Si was found.[22] On the other hand, there is evidence that transformation stasis occurs in an Fe-0.35C-2.27Mn-2.34Si alloy but not in either the Fe-C-Mn or Fe-C-Si alloys with similar alloy concentrations.[5,10,11] The interactions among alloying elements are thus important to the overall transformation behavior, and systematic studies on transformation stasis in multicomponent alloys are needed.

In the present study, austenite decomposition kinetics, primarily to ferrite and carbide, are investigated in four multicomponent steels. An Fe-0.1C-0.4Mn-0.3Si steel is employed as a reference alloy, and the effects of small additions of Ni, Cr, or Mo on overall transformation kinetics are determined.

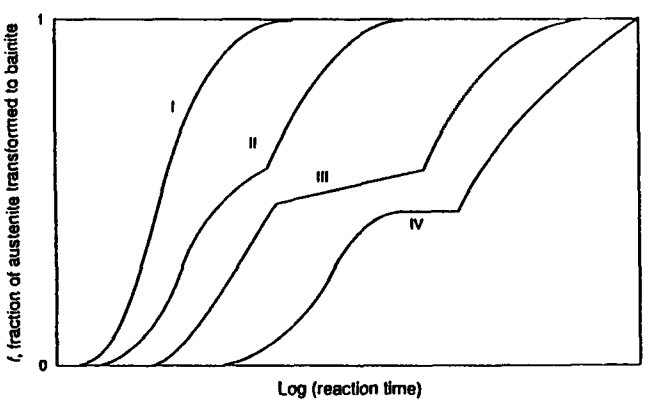

Fig. 1—Four types of transformation behavior observed in Fe-C-X alloys.[1]

II. EXPERIMENTAL PROCEDURE

Alloys for this study were vacuum-induction melted, cast into 35-kg ingots and redundantly hot-worked. Bars 12 × 12 × 150 mm in size were machined from the hot-worked material and homogenized in quartz under 1/3 atm Ar for 3 days at 1250 °C. Carbon combustion analysis was performed on each alloy before and after homogenization to ensure that decarburization did not occur. An Fe-0.1C-0.4Mn-0.3Si (concentrations in weight percent) steel was chosen as a reference alloy. Three additional alloys were made by adding 3Ni, 1Cr, or 0.5Mo to the reference alloy (Table I). Henceforth, these alloys are referred to as the reference, Ni, Cr, and Mo alloys, respectively. The continuous-cooling-transformation (CCT) diagram for each alloy was measured dilatometrically, using 15 cooling rates. Dilatometer samples 3 mm in diameter × 10-mm long were heated to 1200 °C at a rate of 400 °C per minute and held for 15 minutes before cooling.

Homogenized material was cold-rolled and cut into 5 × 5 × 0.38-mm coupons for isothermal heat treatment. These were austenitized at 1200 °C for 15 minutes in a graphite-deoxidized $BaCl_2$ salt bath. Following austenitization, the samples were transferred to a deoxidized lead bath for isothermal reaction. Isothermal transformation was carried out at temperatures between 500 °C and 675 °C, and the reaction time ranged from 1 second to 10,000 seconds (about 3 hours). The samples were then quenched into ice brine. Carbon analysis was also performed after isothermal heat treatment to verify that decarburization did not take place in the austenitizing salt bath or in the lead bath.

Isothermal transformation curves were determined by quantitative metallography.[23,24,25] The fraction of austenite transformed to ferrite (or to ferrite plus carbide) was determined for each transformation time and temperature to within approximately ±2 pct. The etchant used was 5 g $FeCl_3$, 5 drops of HCl, and H_2O to make 100 mL of solution; the etching time was about 10 seconds.[26] This procedure produced good contrast suitable for point counting. An over-etch with 2 pct Nital or an 8 pct sodium metabisulfate etch for 10 seconds, followed by a 2 pct Nital etch for 5 seconds, was used in some cases.[21,27] Both of these methods reveal subgrain boundaries between sympathetically nucleated ferrite plates.

Transmission electron microscope (TEM) specimens were prepared by grinding heat-treated samples to a thickness of 100 μm and punching into 3-mm disks. These were then mechanically dimpled 30-μm deep and jet polished to perforation in a South Bay Model 550C single jet thinning instrument using a 30 pct HNO_3,

Table I. Compositions of the Four Alloys (in Weight Percent)

	C	Mn	Si	X
Reference alloy	0.11	0.41	0.31	—
Ni alloy	0.11	0.42	0.31	3.03 Ni
Cr alloy	0.11	0.41	0.31	0.99 Cr
Mo alloy	0.11	0.42	0.31	0.50 Mo

70 pct methanol solution at −50 °C and 20 to 30 V. Transmission electron microscope observations were carried out with a PHILIPS* EM420 operated at 120 kV.

*PHILIPS is a trademark of Philips Electronic Instruments Corporation, Mahwah, NJ.

III. RESULTS

A. *Kinetics*

The CCT diagrams of the alloys (Figure 2) provided a relatively easy way to select the temperatures and times for isothermal heat treatments. For each alloy, isothermal transformation curves were measured at 500 °C, 550 °C, 600 °C, and 650 °C (and 675 °C for Ni and Mo alloys) for reaction times between 1 second and 10,000 seconds. These temperatures and reaction times were chosen to correspond roughly to the time and temperature range of the discontinuities in the CCT diagrams. The isothermal transformation curves, Figures 3 through 6, were categorized according to the types of behavior shown in Figure 1.

The transformation curves of the reference alloy and the Cr alloy (Figures 3 and 4) exhibit type I curves at all temperatures investigated. Austenite starts to transform in less than 10 seconds, and the transformation proceeds rapidly to completion. Transformation at higher temperatures initiates at longer times and proceeds with slower kinetics. The delay in the start of transformation at higher temperature coincides with the trend in their corresponding CCT initiation curves.

As for Ni and Mo alloys, their isothermal transformation curves (Figures 5 and 6) showed similar shapes as those of the reference and Cr alloys below 600 °C, *i.e.*, type I transformation. However, after 1000 seconds at 650 °C (Figure 5(d)), the Ni alloy exhibits a cessation of transformation at about 75 pct transformation. In the Mo alloy, the transformation curve at 650 °C shows an obvious change in slope at about 18 seconds (log $(t) = 1.25$), and the slope is approximately zero between 18 and 178 seconds (Figure 6(d)). Cessation of transformation at this temperature occurs at a transformation level of 70 pct. Both of these curves are classified as type IV transformation (Figure 1). Transformation curves of 675 °C for Ni and Mo alloy are shown in Figures 5(e) and 6(e), respectively. Transformation cessation is also found in both alloys at 675 °C (Figures 5(e) and 6(e)), with similar transformation levels as found at 650 °C. One apparent difference between the Ni and Mo

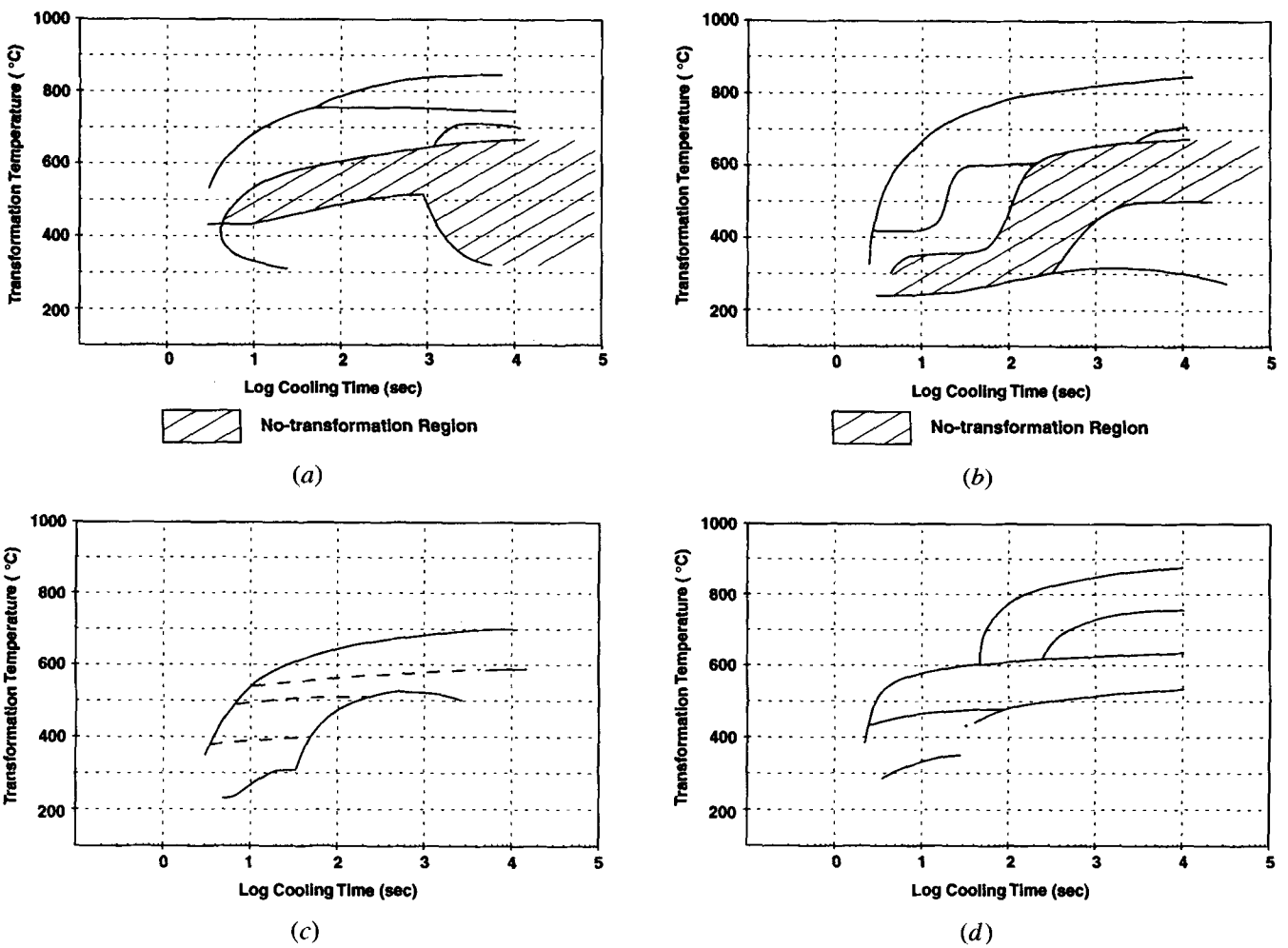

Fig. 2—CCT diagrams for (*a*) the reference alloy, (*b*) the Cr alloy, (*c*) the Ni alloy, and (*d*) the Mo alloy. The curves represent an initiation of transformation or a discontinuity in the overall transformation kinetics.

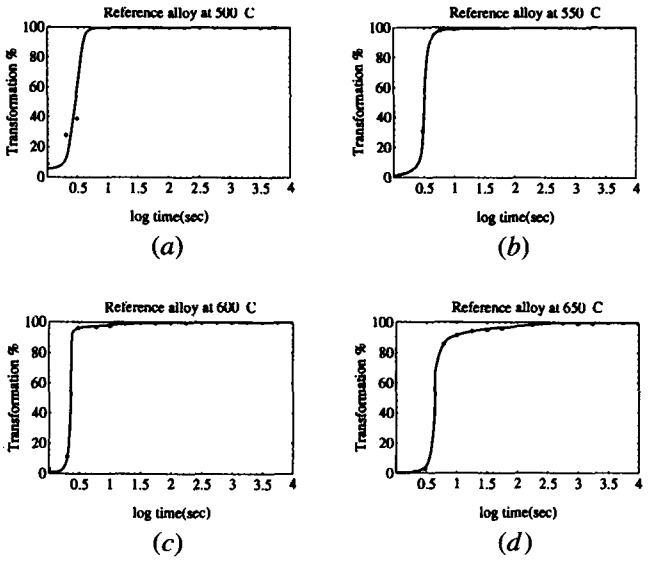

Fig. 3—Overall transformation kinetics of the reference alloy isothermally reacted at (*a*) 500 °C, (*b*) 550 °C, (*c*) 600 °C, and (*d*) 650 °C.

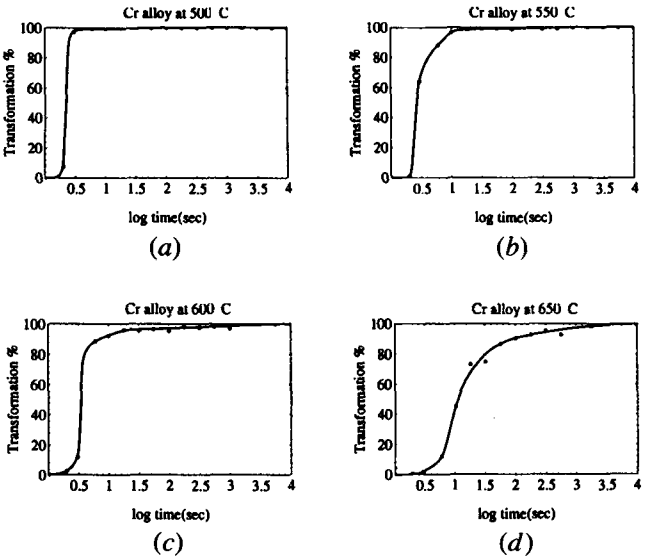

Fig. 4—Overall transformation kinetics of the Cr alloy isothermally reacted at (*a*) 500 °C, (*b*) 550 °C, (*c*) 600 °C, and (*d*) 650 °C.

alloys is that transformation in the Ni alloy does not reach completion within 10,000 seconds at 650 °C and 675 °C, but it does resume following transformation stasis in the Mo alloy and eventually reaches ~95 pct.

The transformation curve of the Mo alloy reacted at 600 °C (Figure 6(c)) shows that the transformation slows at a level of about 93 pct after 100 seconds; however, the shape of this curve appears more like type I than type IV behavior, since the transformation is nearly complete at this level.

B. *Microstructure*

1. *Optical morphology of ferrite and carbides*

Optical micrographs of the proeutectoid ferrite morphology are shown in Figures 7(a) through (d). The general features found in each alloy are considered separately.

The Reference Alloy

Figure 7(a) shows the ferrite morphology of the reference alloy isothermally reacted at 500 °C for 2 seconds. Long ferrite plates consist of an array of smaller sympathetically nucleated crystals.[21] Ferrite sideplates develop extensively in this alloy, and the ferrite plates have a degenerate[28] appearance.

A nonlamellar mixture of carbide and ferrite forms between groups of ferrite crystals (Figure 7(a)). Similar structures in other alloys have been termed "nodular bainite" (Figure 3 of Reference 2 and Figure 1 of Reference 29). For reaction temperatures between 500 °C and 650 °C, nodular bainite forms in less than 10 seconds (Figure 8). At 500 °C, for example, nodular bainite starts to form after approximately 2 seconds or at about 30 pct transformation.

Cr Alloy

The microstructure of the Cr alloy after isothermal reaction at 600 °C for 3 seconds is shown in Figure 7(b).

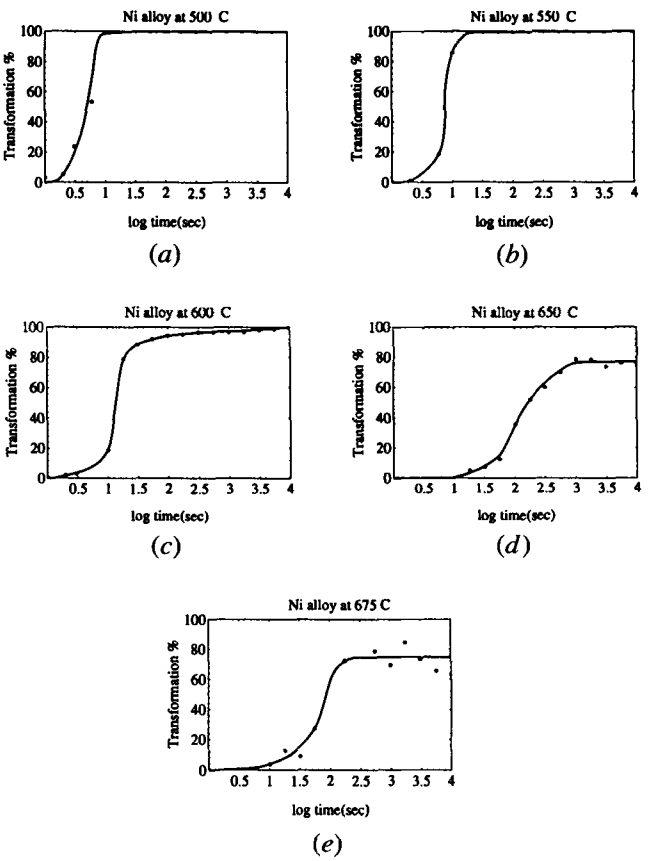

Fig. 5—Overall transformation kinetics of the Ni alloy isothermally reacted at (*a*) 500 °C, (*b*) 550 °C, (*c*) 600 °C, (*d*) 650 °C, and (*e*) 675 °C.

Sympathetically nucleated ferrite appears to dominate the microstructure. The ferrite crystals are thinner and longer than those of the reference alloy, even though the reaction temperature of Figure 7(b) is 100 °C higher than that of Figure 7(a). Figure 9 shows the microstructure of

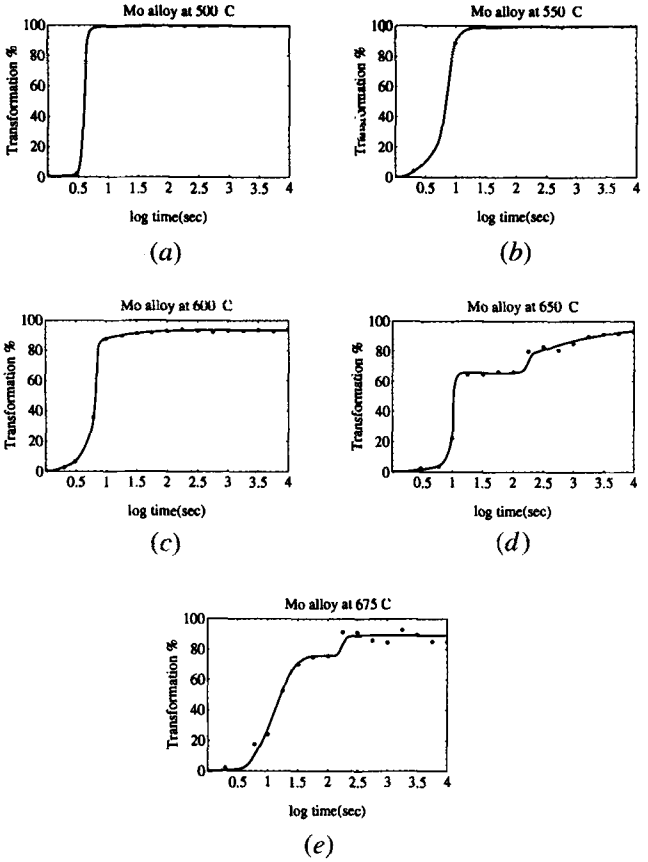

Fig. 6—Overall transformation kinetics of the Mo alloy isothermally reacted at (*a*) 500 °C, (*b*) 550 °C, (*c*) 600 °C, (*d*) 650 °C, and (*e*) 675 °C.

the Cr alloy reacted at 650 °C for 18 seconds. The formation of carbides does not start as early as in the reference alloy, and carbide formation initiates at grain boundaries rather than between ferrite plates. The formation of nodular bainite also occurs at a comparatively higher percentage transformation than in the reference alloy (Figure 7(a)).

Ni Alloy

The morphology of ferrite in the Ni alloy isothermally reacted at 600 °C for 10 seconds is shown in Figure 7(c). Both sympathetically nucleated ferrite plates and grain boundary ferrite appear to be more equiaxed than those found in the reference alloy. Aggregates of sympathetically nucleated ferrite crystals are also found to be comparatively larger than those in the other alloys with the same amount of transformation.

As in the reference alloy, nodular bainite is observed at early stages of transformation at temperatures below 600 °C. Carbides form at about 24 pct transformation or after as little as 3 seconds at 500 °C (Figure 10(a)). At 550 °C and 600 °C, nodular bainite forms after 10 and 18 seconds, respectively. The transformation level where carbides start to form at these temperatures appears to be approximately 60 pct.

Isothermal transformation at 650 °C or 675 °C does not produce carbides in the Ni alloy for reaction times up to 10,000 seconds, and the ferrite morphology is blocky (Figure 10(b)) rather than platelike. The apparent size of the blocky ferrite grains appears to be about 50 μm. It should be noted that cessation of transformation is observed at 650 °C and 675 °C in the Ni alloy at about 70 pct transformation, and the blocky ferrite morphology is present at these temperatures during transformation stasis.

Mo Alloy

The morphology of ferrite in the Mo alloy is shown in Figure 7(d). The ferrite plates appear very degenerate, and the ratio of the ferrite plate length to thickness is larger than that found in the reference and the Ni alloys. Sympathetically nucleated ferrite is the predominant ferrite morphology.

No nodular bainite was found at any temperatures, including those with transformation stasis. The microstructure of the Mo alloy during transformation stasis is shown in Figure 11.

2. *Ferrite morphology under TEM*

The purpose of the TEM work was to determine whether carbides are present during transformation cessation in the Ni and the Mo alloys. Isothermal reaction at 650 °C for 3162 seconds (log (t) = 3.5) was selected for the Ni alloy. The blocky ferrite produced by this heat treatment consists of numerous subgrains several microns in size (Figure 12). Two possible mechanisms might generate such a structure: sympathetic nucleation and polygonization. Although the subgrains are generally misoriented by a few degrees or less and thus resemble a polygonalized structure, the individual subboundaries produce deep cusps in the ferrite/austenite or ferrite/martensite boundaries (Figure 12). These suggest that the sub-boundaries result from sympathetic nucleation, since the low energy associated with low-angle boundaries formed during polygonalization would be expected to produce shallow triple point junctions when they intersect ferrite/solidus austenite boundaries. The small dots in the ferrite grains of the Ni alloy (Figure 12(a)) are similar to those found in the ternary Fe-C-Ni alloy (Figure 8 of Reference 4). Tilting experiments failed to reveal any diffraction spots (Figure 12(b)) that could be associated with a carbide or other precipitate phase. The dots are believed to be small dislocation loops.

The heat treatment for the Mo alloy was 650 °C for 178 seconds (within the range of transformation cessation). Compared with the ferrite morphology of the Ni alloy, the ferrite in the Mo alloy (Figure 13) appears to be less equiaxed, and the boundaries between ferrite grains are more faceted. The ferrite plates in the Mo alloy are also thinner and longer. No carbides were found in either the Ni alloy or the Mo alloy for the conditions chosen in the transformation cessation regimes (Figures 12(b) and 13(b)).

3. *Metastable fraction of ferrite*

To ascertain whether cessation of transformation is thermodynamic or kinetic in origin, it is necessary to determine the metastable fraction of ferrite for each case in which type IV behavior is observed. Several statistical thermodynamic models are available to evaluate the

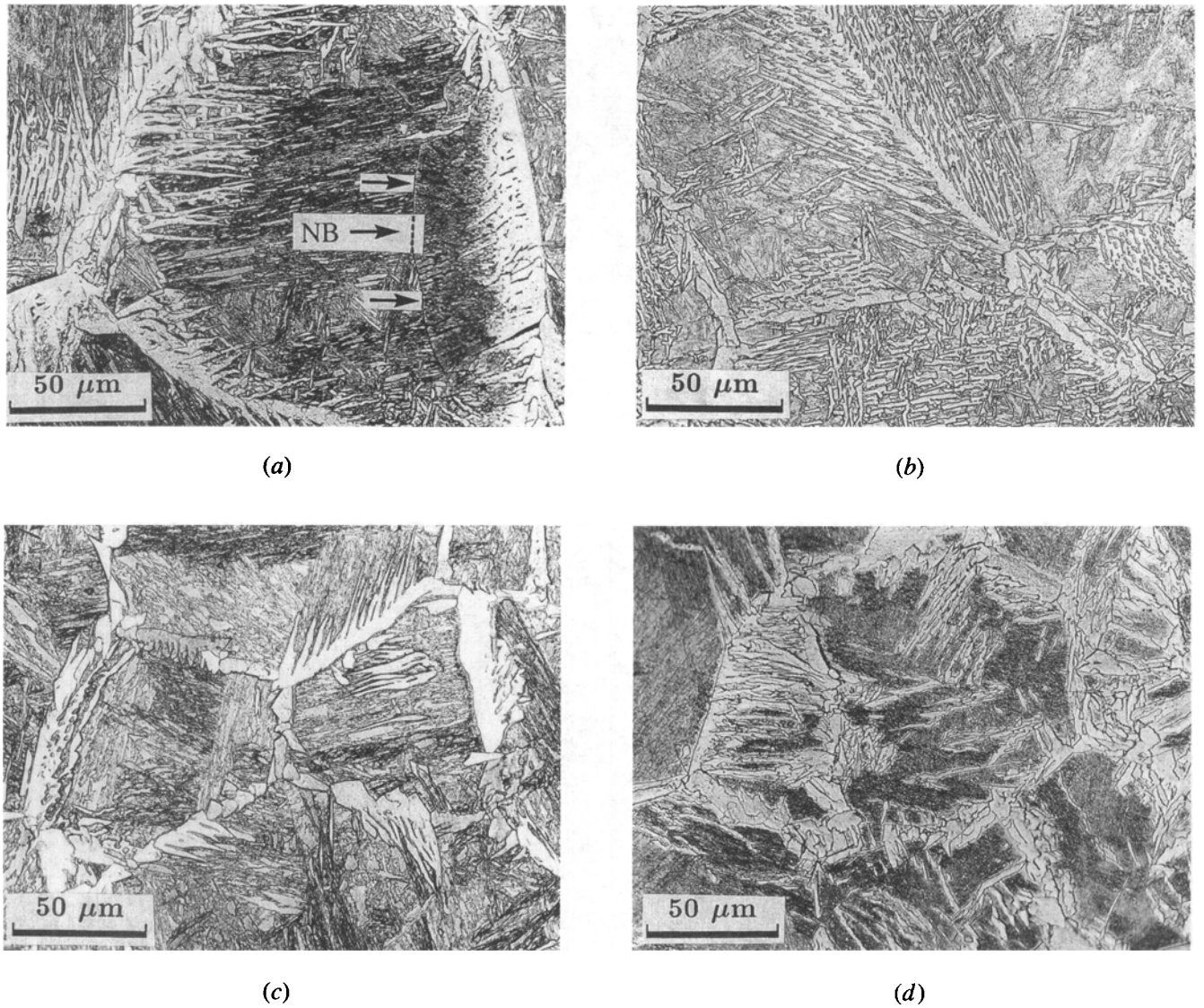

(*a*) (*b*) (*c*) (*d*)

Fig. 7—Morphology of sympathetically nucleated ferrite for (*a*) the reference alloy (reacted at 500 °C for 2 s; NB = nodular bainite), (*b*) the Cr alloy (reacted at 600 °C for 3 s), (*c*) the Ni alloy (reacted at 600 °C for 10 s), and (*d*) the Mo alloy (reacted at 650 °C for 10 s). Etchant: 5 g $FeCl_3$, 5 drops of HCl, with H_2O to make 100 mL.

thermodynamic properties of ferrous alloys. Among them, the quasi-chemical approximation,[30,31] the Hillert–Staffansson[32] model, and the central atoms model by Lupis and Elliott[33] are the most widely used. The central atoms model is selected for this study because the parameters required by the model are readily available or can be derived theoretically from data in the literature,[34,35,36,37] and it is convenient to use for complicated systems.

The $\alpha/(\alpha + \gamma)$ and $\gamma/(\gamma + \alpha)$ tie lines are calculated for each alloy and are used to determine metastable fractions of ferrite in austenite *via* the lever rule. The metastable fractions of ferrite are then compared to the observed fractions of ferrite in cases where transformation ceases before reaching 100 pct.

Two different kinds of equilibrium conditions are considered: orthoequilibrium and paraequilibrium. Under orthoequilibrium,[38] or full equilibrium, the chemical potential of each element is equal in the ferrite and austenite phases. That is:

$$\mu_i^\alpha = \mu_i^\gamma \quad \text{where } i = \text{Fe, C, Mn, Si, or } X \qquad [1]$$

Paraequilibrium[38,39] is a constrained equilibrium in which only the mobile interstitial species (C) is allowed to partition between ferrite and austenite. This type of equilibrium simulates the conditions during ferrite growth from austenite.[15,40,41,42] In materials like Fe-C-Mn-Si-*X* alloys, the ratios of the substitutional alloying elements (Mn, Si, and *X*) to the concentration of the solvent, Fe, are the same in both phases. The paraequilibrium condition can be written for an alloy with t substitutional components as:[43]

$$\mu_C^\alpha = \mu_C^\gamma \qquad [2]$$

$$\mu_{\text{Fe}}^\alpha + \sum_{i=2}^{t} \theta_i \mu_i^\alpha = \mu_{\text{Fe}}^\gamma + \sum_{i=2}^{t} \theta_i \mu_i^\gamma \qquad [3]$$

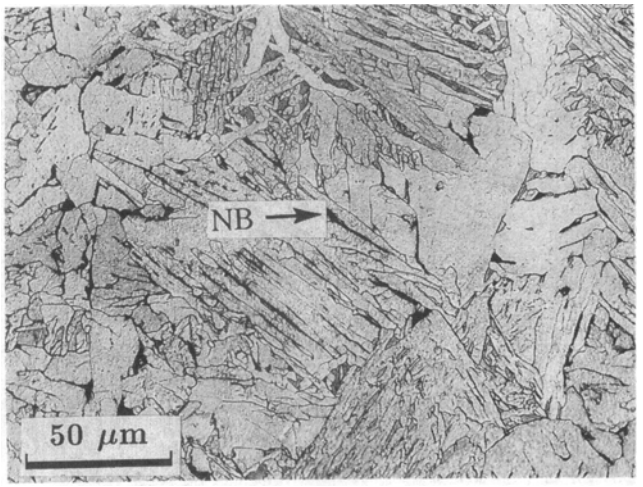

Fig. 8—Carbides are observed in the reference alloy reacted at 650 °C for 10 s. No transformation stasis is found in the transformation curves at any temperatures investigated in this alloy. (NB = nodular bainite).

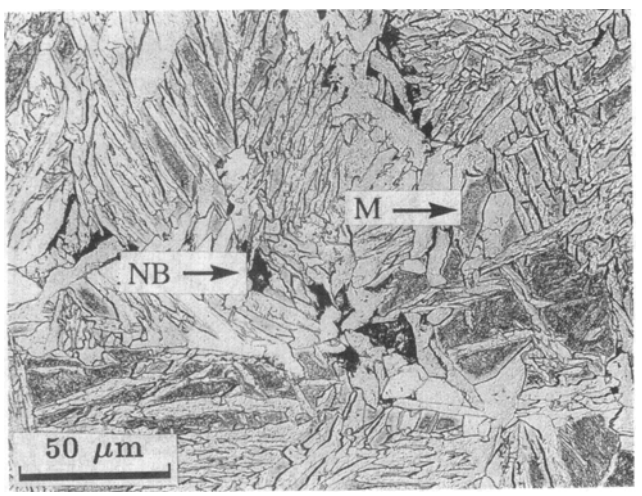

Fig. 9—Microstructure of the Cr alloy reacted at 650 °C for 18 s; carbides start forming at prior austenite grain boundaries. (NB = nodular bainite; M = martensite).

$$\theta_i = \frac{X_i^{\alpha}}{X_{Fe}^{\alpha}} = \frac{X_i^{\gamma}}{X_{Fe}^{\gamma}} \quad (i = 2, 3, \ldots, t) \qquad [4]$$

The total free energy of a mixture of α and γ with the alloy composition is minimized subject to the orthoequilibrium conditions (Eq. [1]) or the paraequilibrium constraints of Eqs. [2] through [4].[44,45] The minimization procedure was performed using the simplex method developed by Nelder and Mead.[46,47,48]

The results of the thermodynamic calculations are listed in Table II. Ortho- and paraequilibrium tie lines between austenite and ferrite were calculated for all the alloys at temperatures between 500 °C and 650 °C. The ferrite fraction increases with decreasing temperature for both ortho- and paraequilibrium, and orthoequilibrium yields a lower metastable fraction of ferrite than paraequilibrium in all alloys except the Cr alloy, for which the orthoequilibrium equations did not converge.

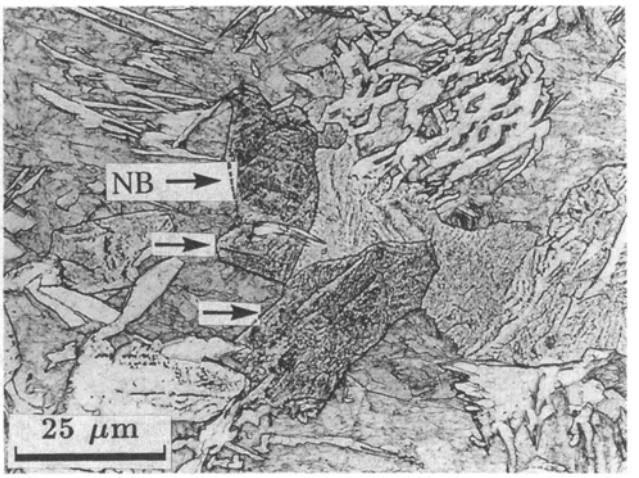

(*a*)

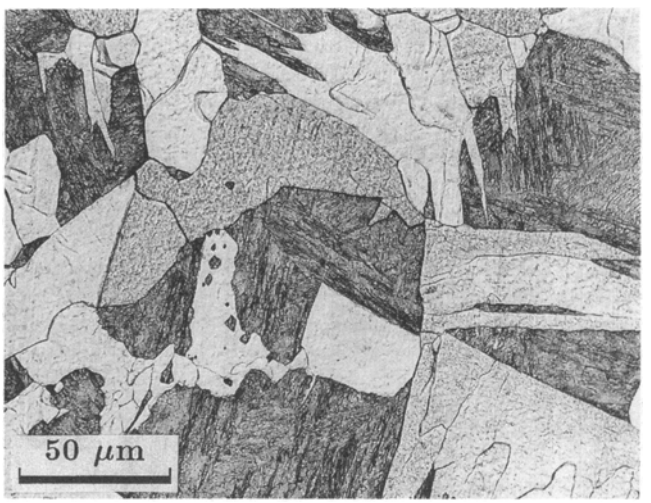

(*b*)

Fig. 10—(*a*) Carbides are found in the microstructure of the Ni alloy when transformation stasis is absent (reacted at 500 °C for 3 s; NB = nodular bainite). (*b*) The microstructure of the Ni alloy during transformation stasis; carbides are absent (reacted at 675 °C for 10,000 s).

The Ni alloy shows the lowest C concentration in the $\gamma/(\gamma + \alpha)$ boundary at all the temperatures investigated. The C concentration in austenite under paraequilibrium in the Ni alloy at 650 °C is about 4.61 at. pct, compared to 6.13, 5.84, and 6.19 at. pct C in the reference, Cr, and Mo alloys, respectively. As a consequence, the paraequilibrium ferrite fraction in the Ni alloy is lower than that of the other alloys.

IV. DISCUSSION

As shown in Figures 2(a) and (b), the CCT diagrams of the reference alloy and the Cr alloy have similar shapes at the initiation of transformation. Although transformation begins slightly later in the Cr alloy, they both have a bay temperature at about 750 °C. The isothermal transformation curves (Figures 3(a) through (d)

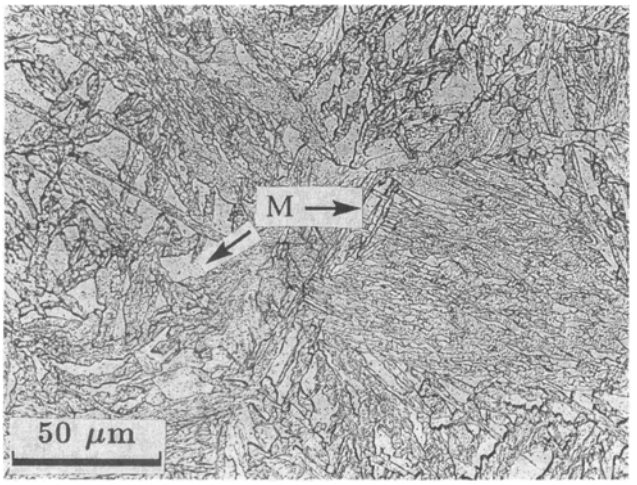

Fig. 11—Carbides are not observed in the Mo alloy during transformation stasis (reacted at 650 °C for 178 s; M = martensite).

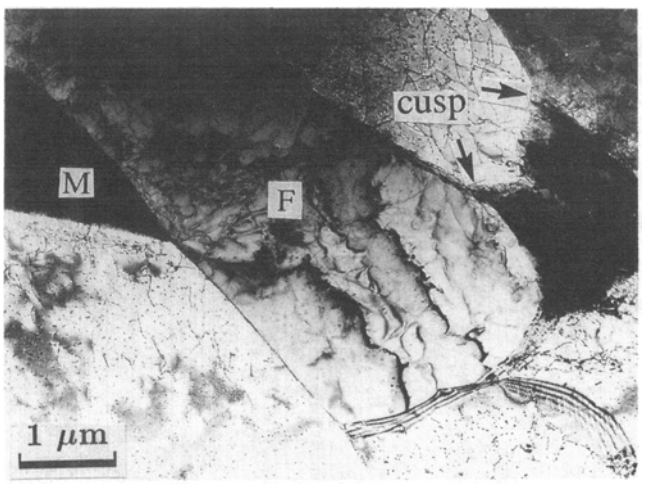

(*a*)

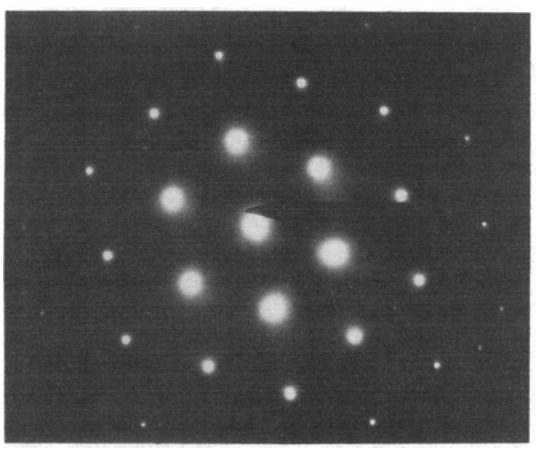

(*b*)

Fig. 12—The morphology of ferrite in the Ni alloy reacted at 650 °C for 3162 s. (*a*) Bright-field TEM and (*b*) diffraction pattern showing absence of carbides during transformation stasis in Ni alloy (M = martensite; F = ferrite).

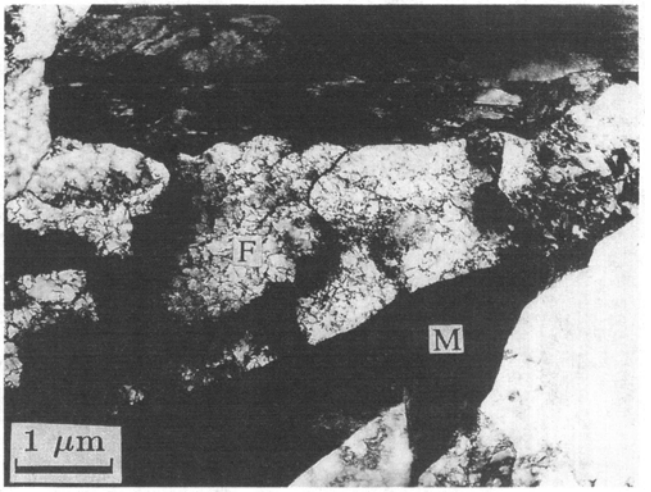

(*a*)

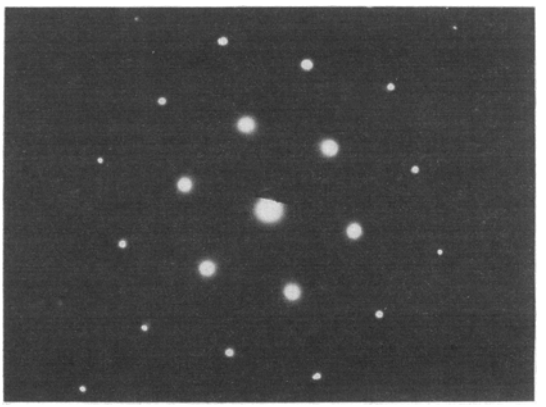

(*b*)

Fig. 13—The TEM morphology of the Mo alloy during transformation stasis (reacted at 650 °C for 178 sec; M = martensite; F = ferrite). (*a*) Bright field and (*b*) diffraction pattern showing absence of carbides.

and 4(a) through (d)) of the reference and Cr alloy are also very much alike. The only apparent difference is for isothermal transformation at 650 °C, at which temperature the Cr alloy transforms slightly more slowly than the reference alloy.

The CCT diagram of the Ni alloy is shown in Figure 2(c). The absence of a distinct discontinuity in the transformation initiation curve of the Ni alloy's CCT diagram at any cooling rate employed prevented identification of a distinct bay temperature. The lack of a discontinuity may be due to an absence of a change in transformation mechanism or to an insufficiently slow cooling rate in the dilatometer. According to Figure 2(c), the time to initiation of transformation increases greatly as the transformation temperature approaches 700 °C. If an upper *C* curve is not revealed as a result of an insufficiently slow cooling rate, 700 °C might thus be a temperature close to T_b. This is supported by the fact that cessation of transformation is found at both 650 °C and 675 °C (Figures 5(d) and (e)).

The CCT diagram of the Mo alloy is shown in

Table II. The Calculated ($\alpha/(\alpha + \gamma)$ and $\gamma/(\gamma + \alpha)$) Tie Lines of the Four Alloys under Orthoequilibrium and Paraequilibrium at 500 °C, 550 °C, 600°C, and 650 °C. (All concentrations are in Atomic Percent.)

Reference Alloy (or Fe-0.46 At. Pct. C-0.40 At. Pct Mn-0.60 At. Pct. Si)

		Orthoequilibrium (At. Pct)					Paraequilibrium (At. Pct)				
Temperature		C	Mn	Si	X	Ferrite (Pct)	C	Mn	Si	X	Ferrite (Pct)
500 °C	$\alpha/(\alpha + \gamma)$	0.10	0.28	0.61	—	—	0.14	0.41	0.60	—	—
	$\gamma(\gamma + \alpha)$	12.35	4.57	0.05	—	97.0	11.95	0.36	0.54	—	97.3
550 °C	$\alpha/(\alpha + \gamma)$	0.11	0.30	0.61	—	—	0.15	0.41	0.60	—	—
	$\gamma(\gamma + \alpha)$	10.19	3.25	0.10	—	96.5	10.03	0.37	0.54	—	96.8
600 °C	$\alpha/(\alpha + \gamma)$	0.11	0.32	0.61	—	—	0.14	0.41	0.60	—	—
	$\gamma(\gamma + \alpha)$	8.10	2.34	0.15	—	95.6	8.09	0.37	0.55	—	96.0
650 °C	$\alpha/(\alpha + \gamma)$	0.11	0.32	0.62	—	—	0.13	0.41	0.60	—	—
	$\gamma(\gamma + \alpha)$	6.06	1.70	0.22	—	94.0	6.13	0.38	0.56	—	94.4

Cr Alloy (or Fe-0.46 At. Pct. C-0.40 At. Pct Mn-0.59 At. Pct. Si-1.07 At. Pct. Cr)

		Orthoequilibrium (At. Pct)					Paraequilibrium (At. Pct)				
Temperature		C	Mn	Si	Cr	Ferrite (Pct)	C	Mn	Si	Cr	Ferrite (Pct)
500 °C	$\alpha/(\alpha + \gamma)$	—	—	—	—	—	0.11	0.41	0.60	1.07	—
	$\gamma(\gamma + \alpha)$	—	—	—	—	—	11.58	0.36	0.54	0.95	96.9
550 °C	$\alpha/(\alpha + \gamma)$	—	—	—	—	—	0.11	0.41	0.60	1.07	—
	$\gamma(\gamma + \alpha)$	—	—	—	—	—	9.70	0.37	0.54	0.97	96.3
600 °C	$\alpha/(\alpha + \gamma)$	0.11	0.33	0.61	0.77	—	0.11	0.41	0.60	1.07	—
	$\gamma(\gamma + \alpha)$	13.25	2.71	0.06	10.63	97.0	7.78	0.37	0.55	0.99	95.4
650 °C	$\alpha/(\alpha + \gamma)$	0.07	0.32	0.62	0.90	—	0.10	0.41	0.60	1.07	—
	$\gamma(\gamma + \alpha)$	6.59	1.67	0.20	3.72	94.0	5.84	0.38	0.56	1.01	93.7

Ni Alloy (or Fe-0.46 At. Pct. C-0.41 At. Pct Mn-0.60 At. Pct. Si-2.84 At. Pct. Ni)

		Orthoequilibrium (At. Pct)					Paraequilibrium (At. Pct)				
Temperature		C	Mn	Si	Ni	Ferrite (Pct)	C	Mn	Si	Ni	Ferrite (Pct)
500 °C	$\alpha/(\alpha + \gamma)$	0.10	0.28	0.61	2.87	—	0.14	0.41	0.60	2.85	—
	$\gamma(\gamma + \alpha)$	11.45	4.23	0.07	1.99	96.8	10.85	0.36	0.53	2.54	97.0
550 °C	$\alpha/(\alpha + \gamma)$	0.10	0.31	0.62	2.80	—	0.13	0.41	0.60	2.85	—
	$\gamma(\gamma + \alpha)$	8.43	2.50	0.13	8.61	96.2	8.82	0.37	0.55	2.60	95.7
600 °C	$\alpha/(\alpha + \gamma)$	0.10	0.32	0.62	2.69	—	0.12	0.41	0.60	2.85	—
	$\gamma(\gamma + \alpha)$	5.75	1.55	0.22	5.03	93.4	6.74	0.38	0.56	2.66	94.8
650 °C	$\alpha/(\alpha + \gamma)$	0.07	0.32	0.63	2.49	—	0.09	0.41	0.60	2.85	—
	$\gamma(\gamma + \alpha)$	3.55	1.05	0.32	5.58	88.7	4.61	0.39	0.57	2.72	91.8
675 °C	$\alpha/(\alpha + \gamma)$	0.06	0.31	0.64	2.34	—	0.08	0.42	0.60	2.85	—
	$\gamma(\gamma + \alpha)$	2.61	0.90	0.37	5.45	84.1	3.50	0.39	0.58	2.75	88.7

Mo Alloy (or Fe-0.46 At. Pct. C-0.41 At. Pct Mn-0.60 At. Pct. Si-0.29 At. Pct. Mo)

		Orthoequilibrium (At. Pct)					Paraequilibrium (At. Pct)				
Temperature		C	Mn	Si	Mo	Ferrite (Pct)	C	Mn	Si	Mo	Ferrite (Pct)
500 °C	$\alpha/(\alpha + \gamma)$	0.10	0.28	0.61	0.25	—	0.16	0.41	0.60	0.30	—
	$\gamma(\gamma + \alpha)$	13.16	4.74	0.06	1.72	97.2	11.96	0.36	0.53	0.26	97.4
550 °C	$\alpha/(\alpha + \gamma)$	0.12	0.31	0.61	0.27	—	0.16	0.41	0.60	0.29	—
	$\gamma(\gamma + \alpha)$	10.58	3.33	0.10	1.00	96.7	10.06	0.37	0.54	0.26	97.0
600 °C	$\alpha/(\alpha + \gamma)$	0.12	0.32	0.61	0.27	—	0.16	0.41	0.60	0.29	—
	$\gamma(\gamma + \alpha)$	8.31	2.37	0.15	0.63	95.9	8.14	0.37	0.55	0.27	96.1
650 °C	$\alpha/(\alpha + \gamma)$	0.12	0.32	0.63	0.28	—	0.14	0.41	0.60	0.29	—
	$\gamma(\gamma + \alpha)$	6.19	1.72	0.22	0.43	94.3	6.19	0.38	0.56	0.27	94.6
675 °C	$\alpha/(\alpha + \gamma)$	0.11	0.32	0.62	0.28	—	0.12	0.41	0.60	0.29	—
	$\gamma(\gamma + \alpha)$	5.15	1.47	0.26	0.37	92.9	5.20	0.39	0.57	0.28	93.3

Figure 2(d). The discontinuity in the slope of the transformation initiation curve occurs at approximately 625 °C. Transformation cessation (Figures 6(d) and (e)), however, is found in the Mo alloys isothermally reacted at 650 °C and 675 °C, somewhat higher than the CCT bay temperature. Since the CCT diagrams generally lie at lower temperature than TTT diagrams, the T_b in the TTT diagram is probably higher than 625 °C. Thus, cessation of transformation in the Mo alloy at 675 °C may still be transformation stasis below T_b in the TTT diagram.

Near-transformation cessation is observed in the transformation curve of the Mo alloy reacted at 600 °C (Figure 6(c)). The transformation fraction remains at a

level of 93 vol pct after approximately 100 seconds. As shown in Figure 2(d), the flat secondary curve in the Mo alloy's CCT diagram indicates that the transformation is sluggish at temperatures between 500 °C and 625 °C.

At temperatures between 500 °C and 550 °C, a delay in the start of transformation (Figures 5(a) and (b)) is found in the Ni alloy relative to that in the Mo alloys (Figures 6(a) and (b)). A similar trend can be observed in the initiation curves of their CCT diagrams.

In the CCT diagrams of the reference and Cr alloys, the dilatometric measurements exhibit several regions of apparent transformation stasis, but transformation stasis is not observed in these alloys in isothermal transformation experiments. On the other hand, cessation of transformation is found in the Ni and Mo alloys at temperatures above 650 °C, but a transformation stasis region is not found in either of their CCT diagrams. Thus, as was noted many years ago,[49] dilatometric experiments can sometimes give qualitatively different results from those obtained with isothermal heat treatments and quantitative metallography.

To be interpreted as transformation stasis, transformation of austenite to ferrite must cease before the metastable fraction of ferrite is achieved.[1] In the present study, paraequilibrium is employed to interpret the metastable stasis level. Among the possible stasis observations, cessation of transformation in the Mo alloy reacted at 600 °C (Figure 6(c)) can be eliminated as an occurrence of transformation stasis, since the percent transformed (93 vol pct) is approximately the same as the paraequilibrium metastable amount of ferrite (96 at. pct, Table II).*

*Volume and atomic percentages are equivalent to within the limits of experimental and calculation error.

However, cessation of transformation occurs at about 75 vol pct at both 650 °C and 675 °C in Ni alloy (Figures 5(d) and (e)), and the paraequilibrium ferrite fractions are considerably higher (92 and 89 at. pct, respectively). The Mo alloy stops transforming at about 70 pct at 650 °C and 675 °C (Figures 6(d) and (e)), but the calculated paraequilibrium ferrite fractions are 95 and 93 pct, respectively (Table II). The calculated values are significantly higher than the experimental values in these cases, so the cessation of transformation found in the Ni and Mo alloys at 650 °C and 675 °C does not correspond to the metastable fraction of ferrite. The plateau found in the transformation curves of these alloys and temperatures can thus be recognized as transformation stasis.

The SDLE was originally proposed by Kinsman and Aaronson[11,18] to explain sluggish ferrite growth kinetics in steels containing specific alloying elements. It maintains that these alloying elements are swept up by ferrite/austenite boundaries in a nonequilibrium fashion and reduce the activity of C in austenite such that the effective concentration gradient in austenite driving growth is diminished. Although a quantitative SDLE theory is unavailable, and a direct test of the hypothesis has not been done, a number of indirect experiments and observations support the basic concept.[2,4,13] In the context of the present experiment, the SDLE can be used to explain the presence of transformation stasis. The mechanism through which the SDLE causes transformation stasis is described in several recent reviews.[13,19]

For alloys containing elements producing a strong SDLE, the segregated alloying elements at ferrite/austenite boundaries impede ferrite growth enough that renucleation of ferrite is necessary for overall transformation to proceed. Renucleation requires sufficient undercooling to allow sympathetic nucleation of ferrite. Sympathetic nucleation continues until the surrounding austenite becomes sufficiently enriched in C to prevent further ferrite nucleation. Transformation stasis then begins, since overall transformation effectively ceases when both nucleation and growth of ferrite stop. The transformation does not resume until carbide precipitation or the volume diffusion of the substitutional species relieves the SDLE on ferrite/austenite boundaries.

In order to test the applicability of this hypothesis to the present alloys, the microstructures during transformation stasis were investigated with optical microscope and TEM. As shown in Figures 10(b), 11, 12, and 13, carbides are not present in either the Ni alloy or the Mo alloy during transformation stasis. In contrast, carbide precipitation occurs during the early stages of transformation in the Cr and reference alloys, and these steels do not exhibit transformation stasis (Figures 8 and 9). In addition, carbides form in the Ni alloy at temperatures that do not produce transformation stasis (Figure 10(a)). These observations are consistent with the model for transformation stasis based on the SDLE hypothesis.

Previous work in Fe-C-X alloys indicates that transformation stasis occurs at 555 °C in Fe-0.13C-2.99Cr,[3] below T_b and above minimum threshold concentrations of C and Mo in Fe-C-Mo alloys,[2] and at 550 °C in Fe-0.1C-2.99Mn.[4] Transformation stasis was not observed in several Fe-C-Ni or Fe-C-Si alloys nor in an Fe-0.38C-3.11Mn alloy. For the current hypothesis, the appearance of stasis requires: (1) a strong SDLE to inhibit ferrite growth and (2) the absence of carbide formation. The latter condition ensures that the C content of untransformed austenite increases during ferrite growth, thereby suppressing sympathetic nucleation of ferrite.

For the most recent model for the SDLE,[2] a solute draglike effect results when the chemical potential of C in the ferrite/austenite boundary is significantly less than the paraequilibrium value. Predicting this condition requires knowledge of the boundary concentrations of C and the solute species and a thermodynamic description of the boundary. Since very little of this information is available, one must resort to generalities. It is likely, as has been suggested before,[1,15] that elements capable of reducing the C activity should produce an SDLE. The elements Mo, Mn, and Cr, whose interaction parameters with C are negative, should thus produce an SDLE, and Ni and Si, whose interaction parameters are positive, should not.

In an alloy with more than one alloying element, interactions among the substitutional species in the ferrite/austenite boundary must also be considered. Of the quaternary steels, Fe-C-Mn-Si has received the most attention. Bhadeshia and Edmonds[9] claim that Fe-0.43C-3.00Mn-2.12Si shows transformation stasis. As described previously, both Fe-0.38C-3.11Mn and Fe-0.38C-1.73Si[5] steels do not exhibit transformation

stasis (Table III). However, the methods and results of Reference 9 have been challenged on experimental grounds and are thus not definitive.[5,6] Chen and coworkers[10] appear to have identified transformation stasis in Fe-0.35C-2.27Mn-2.34Si reacted between 450 °C and 535 °C. Thus, the interactions of Mn and Si could produce transformation stasis. The large temperature range over which stasis is found suggests that Si enhances the SDLE when combined with Mn. This possibility has been suggested to result from enhanced Mn segregation to ferrite/austenite boundaries caused by Si.[5] It is also likely that inhibition of cementite formation by Si at higher C concentrations (0.35C) in Fe-C-Si-Mn alloys encourages the development of transformation stasis.

Since Fe-C-Mn-Si alloys exhibit stasis under some conditions, the absence of transformation stasis in the reference alloy may be a consequence of the low concentrations of C, Mn, and Si in the alloy (Table III). That is, these elements are below the threshold[2] concentrations for the Fe-C-Mn-Si system.

Transformation curves for an Fe-0.12C-3.28Ni alloy isothermally reacted at 650 °C and 675 °C were also determined (Figure 14) to extend the temperature range of data obtained in a previous study.[4] These results indicate that transformation stasis is absent in this alloy at temperatures between 550 °C and 675 °C.[4] Therefore, the interactions among Mn, Si, and Ni, rather than the Ni addition *per se*, lead to transformation stasis in the Ni alloy (Table III). The addition of Ni to the reference alloy apparently lowers T_b from 750 °C in the reference alloy to 700 °C. This decrease could be related to the fact that Ni is an austenite stabilizer. The reduction in driving force for ferrite formation caused by Ni could, in effect, lower the threshold concentrations of C, Mn, and Si required to cause transformation stasis.

The reduction in driving force for ferrite precipitation engendered by Ni may also explain the differences in the microstructures of the Ni alloy from the other alloys studied. Two features are found in the microstructure survey of the Ni alloy: the grain boundary ferrite at the early stage of transformation is relatively thicker than the other alloys studied (Figure 7(c)), and blocky ferrite is formed during transformation stasis (Figure 10(a)). Since the driving force for ferrite formation is decreased by Ni, sympathetically nucleated ferrite is comparatively more difficult to form than in the other alloys.

In contrast to an Ni addition, Mo is a ferrite stabilizer[50] and increases the driving force for ferrite precipitation. However, it also produces a strong SDLE, as is evidenced by the anomalously slow ferrite growth kinetics[1] and transformation stasis[2] in Fe-C-Mo alloys (Table IV). Since transformation stasis is not found in an Fe-0.13C-0.46Mo steel[2] and the reference alloy, the combined effects of Mo, Mn, and Si in the Mo alloy result in transformation stasis at substantially lower threshold concentrations of C and Mo than required to produce stasis in a ternary Fe-C-Mo alloy.

V. CONCLUSIONS

The overall kinetics of proeutectoid ferrite transformation were investigated in a series of Fe-0.1C-0.4Mn-0.3Si-*X* alloys, where *X* stands for 3Ni, 1Cr, or 0.5Mo.

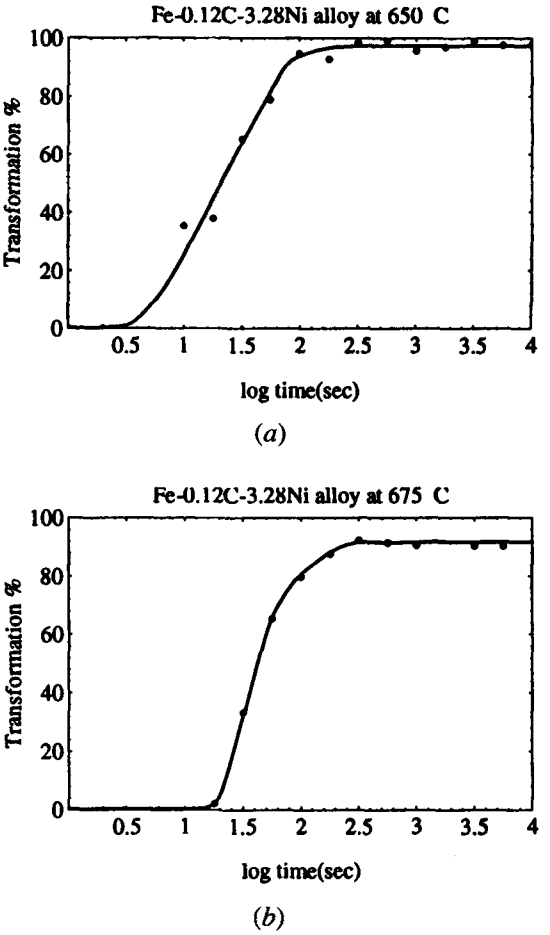

Fig. 14—Overall transformation kinetics of an Fe-0.12C-3.28Ni alloy isothermally reacted at (*a*) 650 °C and (*b*) 675 °C.

An Fe-0.1C-0.4Mn-0.3Si served as a reference alloy for comparisons. At temperatures between 500 °C and 650 °C, no transformation stasis is found in the reference and the Cr alloys. Transformation stasis is observed at 650 °C and 675 °C in the Ni alloy and in the Mo alloy. The fraction of ferrite present during transformation stasis is significantly less than the calculated metastable (paraequilibrium) fraction of ferrite at these isothermal reaction temperatures.

Transformation stasis was not observed under conditions that result in carbide precipitation. Carbides do not form for the reaction temperatures and times in the stasis regime of the Ni and the Mo alloys. However, carbide precipitation does occur in the Ni alloy at lower temperatures where transformation stasis is absent. Stasis is also absent in the reference and the Cr alloys, and these alloys exhibit extensive carbide precipitation.

The transformation kinetics in these alloys are consistent with a previously proposed explanation for transformation stasis.[2] Transformation stasis occurs in alloys containing sufficient concentrations of C and solute elements that produce a strong solute draglike effect, as long as carbide precipitation is absent. At large driving forces for ferrite formation, ferrite precipitates *via* sympathetic nucleation, with subsequent growth severely restricted by the solute draglike effect.

The presence of transformation stasis is encouraged in

Table III. Transformation Stasis and Interactions of Mn, Si, and Ni

Alloys (Wt Pct)	C	Mn	Si	*X*	Stasis	Reference
Fe-C-Mn-Si	0.35	2.27	2.34	—	Yes	10
Fe-C-Mn	0.38	3.11	—	—	No	5
Fe-C-Si	0.38	—	1.73	—	No	5
Fe-C-Mn-Si	0.11	0.41	0.31	—	No	this work
Fe-C-Mn-Si-Ni	0.11	0.42	0.31	3.03 Ni	Yes	this work
Fe-C-Ni	0.12	—	—	3.28 Ni	No	4, this work

Table IV. Transformation Stasis and Interactions of Mn, Si, and Mo

Alloys (Wt Pct)	C	Mn	Si	*X*	Stasis	Reference
Fe-C-Mn-Si-Mo	0.11	0.42	0.31	0.50 Mo	Yes	this work
Fe-C-Mn-Si	0.11	0.41	0.31	—	No	this work
Fe-C-Mo	0.13	—	—	0.46 Mo	No	2

the Mo alloy by the combined presence of Mn and Si. Both Mn and Mo may be segregating to ferrite-solidus austenite boundaries to produce an enhanced SDLE, and Si simultaneously suppresses carbide formation.

In the Ni alloy, the temperatures with transformation stasis are within 50 °C below the CCT bay temperature. Stasis in this alloy is probably due to a reduction in the threshold concentrations of C, Si, and Mn required for stasis, since Ni greatly reduces the driving force for ferrite formation.

Even though the reference and the Cr alloys have similar CCT curves as the Ni alloy, transformation stasis is not observed in these alloys because of the formation of carbides. It may also be that these alloys are not above the threshold concentrations of C, Mn, Si (and Cr) required to produce transformation stasis.

Some regions in the CCT diagrams of the reference and Cr alloys show no transformation according to dilatometric data. No such regions are found in the CCT diagrams of the Ni and Mo alloys. However, transformation stasis does occur in the Ni and the Mo alloys during isothermal transformation but not in the reference and Cr alloys.

ACKNOWLEDGMENTS

The financial support of the Ford Motor Company, through the offices of N.A. Gjostein, is gratefully acknowledged. The authors would also like to thank J.D. Defilippi, USX Corporation, for providing the alloys, W. King of the Naval Research Laboratory for performing the dilatometric measurements, and W.H. Clements II for assistance with the heat treatments.

REFERENCES

1. G.J. Shiflet and H.I. Aaronson: *Metall. Trans. A*, 1990, vol. 21A, pp. 1413-32.
2. W.T. Reynolds, Jr., F.Z. Li, C.K. Shui, and H.I. Aaronson: *Metall. Trans. A*, 1990, vol. 21A, pp. 1433-63.
3. H. Goldenstein and H.I. Aaronson: *Metall. Trans. A*, 1990, vol. 21A, pp. 1465-78.
4. W.T. Reynolds, Jr., S.K. Liu, F.Z. Li, S. Hartfield, and H.I. Aaronson: *Metall. Trans. A*, 1990, vol. 21A, pp. 1479-91.
5. S.K. Liu, W.T. Reynolds, Jr., H. Hu, G.J. Shiflet, and H.I. Aaronson: *Metall. Trans. A*, 1985, vol. 16A, pp. 457-66.
6. H.I. Aaronson, W.T. Reynolds, Jr., H. Hu, and S.K. Liu: *Metall. Trans. A*, 1989, vol. 20A, pp. 324-30.
7. R.F. Hehemann and A.R. Troiano: *Met. Prog.*, 1956, vol. 70, pp. 97-104.
8. W.T. Griffiths, L.B. Pfeil, and N.P. Allen: in *2nd Report of Alloy Steels Research Committee*, The Iron and Steel Institute, London, 1939, pp. 1343-67.
9. H.K.D.H. Bhadeshia and D.V. Edmonds: *Metall. Trans. A*, 1979, vol. 10A, pp. 895-907.
10. G. Chen, H.I. Aaronson, S.K. Liu, and S.S. Brenner: Carnegie Mellon University, Pittsburgh, PA, unpublished research, 1989.
11. H.I. Aaronson: in *The Mechanism of Phase Transformation in Crystalline Solids*, Institute of Metals, London, 1968, pp. 270-81.
12. R.F. Hehemann, K.R. Kinsman, and H.I. Aaronson: *Metall. Trans.*, 1972, vol. 3, pp. 1077-94.
13. H.I. Aaronson, W.T. Reynolds, Jr., G.J. Shiflet, and G. Spanos: *Metall. Trans. A*, 1990, vol. 21A, pp. 1343-80.
14. K.R. Kinsman, E. Eichen, and H.I. Aaronson: *Metall. Trans.*, 1971, vol. 2, pp. 346-48.
15. J.R. Bradley and H.I. Aaronson: *Metall. Trans. A*, 1981, vol. 12A, pp. 1729-41.
16. P.G. Boswell, K.R. Kinsman, G.J. Shiflet, and H.I. Aaronson: in *Mechanical Properties and Phase Transformations in Engineering Materials*, S.D. Antolovich, R.O. Ritchie, and W.W. Gerberich, eds., TMS-AIME, Warrendale, PA, 1986, pp. 445-66.
17. H. Tsubakino and H.I. Aaronson: *Metall. Trans. A*, 1987, vol. 18A, pp. 2047-60.
18. K.R. Kinsman and H.I. Aaronson: in *The Transformation and Hardenability in Steels*, Climax Molybdenum Company, Ann Arbor, MI, 1967, p. 39.
19. W.T. Reynolds, Jr., H.I. Aaronson, and G. Spanos: *Mater. Trans., Jpn. Inst. Met.*, 1991, vol. 32, pp. 737-46.
20. Y. Ohmori and T. Maki: *Mater. Trans., Jpn. Inst. Met.*, 1991, vol. 32, pp. 631-41.
21. H.I. Aaronson and C. Wells: *Trans. AIME*, 1956, vol. 8, pp. 1216-23.
22. T. Tanaka: Ph.D. Thesis, Carnegie Mellon University, Pittsburgh, PA, 1992.
23. E.E. Underwood: *Quantitative Stereology*, Addison-Wesley, Reading, MA, 1979.
24. E.R. Weibel: *Stereological Methods, V.1 Practical Methods for Biological Morphometry*, Academic Press, London, 1979.
25. T. Gladman and J.H. Woodhead: *J. Iron Steel Inst.*, 1960, vol. 194, pp. 189-93.
26. G.F. Vander Voort: *Metallography—Principles and Practice*, McGraw-Hill, New York, NY, 1984.
27. C.K. Shui, W.T. Reynolds, Jr., G.J. Shiflet, and H.I. Aaronson: *Metallography*, 1988, vol. 21, pp. 91-102.
28. H.I. Aaronson, T. Furuhara, J.M. Rigsbee, W.T. Reynolds, Jr., and J.M. Howe: *Metall. Trans. A*, 1990, vol. 21A, pp. 2369-409.
29. W.T. Reynolds, Jr., F.Z. Li, C.K. Shui, G.J. Shiflet, and H.I.

Aaronson: in *Phase Transformations '87*, G.W. Lorimer, ed., Institute of Metals, Cambridge, United Kingdom, 1987, pp. 330-33.
30. E.A. Guggenheim: *Mixtures*, Oxford University Press, Oxford, United Kingdom, 1952.
31. R.H. Fowler and E.A. Guggenheim: *Statistical Thermodynamics*, MacMillan, New York, NY, 1939.
32. M. Hillert and L.I. Staffansson: *Acta Chem. Scand.*, 1970, vol. 24, pp. 3618-26.
33. C.H.P. Lupis and J.F. Elliott: *Acta Metall.*, 1967, vol. 15, pp. 265-76.
34. E. Foo and C.H.P. Lupis: *Acta Metall.*, 1973, vol. 21, pp. 1409-30.
35. C.H.P. Lupis and J.F. Elliott: *Acta Metall.*, 1966, vol. 14, pp. 529-38.
36. C.H.P. Lupis and J.F. Elliott: *Acta Metall.*, 1966, vol. 14, pp. 1019-32.
37. M. Enomoto and H.I. Aaronson: *CALPHAD*, 1985, vol. 9, pp. 43-58.
38. A. Hultgren: *Trans. ASM*, 1947, vol. 39, p. 915.
39. M. Hillert: Technical Report, Swedish Institute for Metals Research, Stockholm, Sweden, 1953.
40. W.T. Reynolds, Jr., M. Eomoto, and H.I. Aaronson: in *Phase Transformations in Ferrous Alloys*, A.R. Marder and J.I. Goldstein, eds., TMS-AIME, Philadelphia, PA, 1983, pp. 155-200.
41. H.I. Aaronson and H.A. Domian: *Trans. TMS-AIME*, 1966, vol. 236, pp. 781-96.
42. M. Enomoto and H.I. Aaronson: *Metall. Trans. A*, 1987, vol. 18A, pp. 1547-57.
43. J.B. Gilmour, G.R. Purdy, and J.S. Kirkaldy: *Metall. Trans.*, 1972, vol. 3, pp. 1455-64.
44. M. Hillert: in *Hardenability Concepts with Applications to Steel*, D.V. Doane and J.S. Kirkaldy, eds., TMS-AIME, Warrendale, PA, 1978, pp. 5-27.
45. J.F. Counsell, E.B. Lees, and P.J. Spencer: *Metal Sci. J.*, 1971, vol. 5, pp. 210-13.
46. J.A. Nelder and R. Mead: *Computer J.*, 1965, vol. 7, pp. 308-13.
47. M.J.D. Powell: *Computer J.*, 1964, vol. 7, pp. 155-62.
48. H. Rosenbrock: *Computer J.*, 1960, vol. 3, pp. 175-84.
49. H.A. Smith: *Trans. AIME*, 1935, vol. 116, pp. 342-62.
50. B. Uhrenius: in *Hardenability Concepts with Applications to Steel*, D.V. Doane and J.S. Kirkaldy, eds., TMS-AIME, Warrendale, PA, 1978, pp. 28-81.